Graphene devices with bottom-up contacts by area-selective atomic layer deposition

Graphene devices with bottom-up contacts by area-selective atomic layer deposition

Nick F.W. Thissen[*,1], *René H.J. Vervuurt*[1], *Adriaan J.M. Mackus*[1], *Johannes J.L. Mulders*[2], *Jan-Willem Weber*[1], *Wilhelmus M.M. Kessels*[1] *and Ageeth A. Bol*[*,1]

[1]Department of Applied Physics, Eindhoven University of Technology, P.O. Box 513, 5600 MB Eindhoven, NL

[2]FEI Electron Optics, Achtseweg Noord 5, 5600 KA Eindhoven, The Netherlands

Keywords: graphene, field-effect transistor, resist residue, atomic layer deposition, area-selective, coupling strength, contact induced doping, metal induced doping, contact resistance

* Authors to whom correspondence should be addressed. E-mail: n.f.w.thissen@tue.nl and a.a.bol@tue.nl.

Abstract

Graphene field-effect transistor devices were fabricated using a bottom-up and resist-free method, avoiding common compatibility issues such as contamination by resist residues. Large-area CVD graphene sheets were structured into device channels by patterning with a focused ion beam. Platinum contacts were then deposited by direct-write atomic layer deposition (ALD), which is a combination between electron beam induced deposition (EBID) and bottom-up area-selective ALD. This is a unique approach that enables nucleation of Pt ALD on graphene, and therefore these devices are the first reported graphene devices with contacts deposited by ALD. Electrical characterization of the devices confirms ambipolar transistor behaviour with typical field-effect mobilities in the range of 1000 – 1800 $cm^2\ V^{-1}s^{-1}$. We observe clear signs of strong Pt-graphene coupling and contact induced hole doping, implying good contact properties in contrast to the conventionally weak bonding between Pt and graphene. We attribute these observations to the reduced amount of resist residue under the contacts, the improved wettability of the Pt due to the use of ALD, and the formation of a graphitic interlayer that bonds the Pt more strongly to the graphene. We conclude that direct-write ALD is a very suitable technique for metallization of graphene devices and to study the intrinsic properties of metal-graphene contacts in more detail. In addition, it offers unique opportunities to control the metal-graphene coupling strength.

The unique electronic properties of graphene have received considerable attention and make it an exciting material as the channel for nanoelectronic devices.[1–5] Despite its promising properties, the formation of good electrical contacts to graphene remains a key bottleneck for many applications even though a substantial amount of research has been devoted to this subject.[6–15] Due to its atomically thin nature, the graphene underneath metal electrodes can be heavily modified. For example, the density of states (DOS) of the graphene under the contacts can deviate from the typical Dirac cone found in pristine graphene, especially when the metal-graphene coupling strength is large.[16–19] At the same time, a difference in work function between the metal and graphene results in contact-induced doping of the graphene,[7,9,19–25] increasing the number of conduction modes under the contacts.[9] The combination of the DOS modification and contact-induced doping effects largely control the electronic transport through metal-graphene interfaces, and they depend on the work function of the metal,[18,20,21] the metal-graphene distance[20,21] and the wettability of the metal.[26]

Even though it is clear that the metal-graphene interface is crucially important, this interface is often contaminated with resist residues originating from the processing of the graphene into devices. The fabrication of devices from large areas of graphene comprises patterning of the graphene to define the channel region, and metallization to form the contacts. Both the patterning and metallization conventionally include photolithography or electron-beam lithography steps in which the graphene must be covered by a resist film. However, removal of the resist film is a real challenge and a residue of the resist is known to remain on the graphene after processing.[27,28] The resist residue is an uncontrolled processing by-product and can drastically alter the metal-graphene interface, e.g. by influencing the metal-graphene distance and metal wettability. As a result it controls the metal-graphene coupling strength and contact-induced doping[19] and has been shown to increase contact resistance.[29–31]

Performance of graphene devices may be improved by using alternative patterning and metallization schemes, which avoid the use of resist films and offer better control over the metal-graphene interface properties. For example, earlier we have shown that direct cutting of the graphene by a focused ion beam is a viable alternative to conventional patterning techniques.[32] A Ga ion beam can be used to make thin cuts in the graphene to electrically isolate device channel regions without using any resist films. For alternative metallization schemes, atomic layer deposition (ALD) has been proposed as a technique for ideal metal-graphene contacts as it improves the morphology of the metal.[9] However, due to the chemical inertness of the graphene, nucleation of the ALD films is very problematic. ALD films on graphene are usually not closed as the metal(oxide) films nucleate preferentially on defects and grain boundaries.[33–35] Moreover, the combination of conventional lithography and ALD introduces significant challenges such as reflowing of the resist films at the temperatures required for metal ALD.[36] Both issues can be avoided by using *direct-write ALD*, which is a previously introduced technique that allows *bottom-up* deposition of ALD contacts.[37–39] Briefly, direct-write ALD combines the direct-write patterning technique of electron-beam induced deposition (EBID) with ALD to fabricate high-quality platinum (Pt) structures without the need for conventional lithography, resist films or lift-off steps. A thin seed layer of Pt/C is first deposited directly in the desired shape by EBID. An area-selective ALD process then transforms the seed layers into pure Pt structures by depositing Pt only on the seed layers (and not on the surrounding substrate) while it simultaneously purifies the seed layers by combusting the carbon in the oxygen half-cycles. Note that the EBID Pt/C material itself has a very high resistivity[40] of more than 10^6 μΩ cm (which makes it unsuitable as contact material directly), while direct-write ALD Pt structures exhibit a near-bulk Pt resistivity[38] of 11 ± 2 μΩ cm. By applying this technique for the deposition of graphene contacts, we can significantly reduce the

amount of resist residue under the contacts and on the graphene channel and study the intrinsic properties of metal-graphene interfaces carefully.

In this work, we demonstrate graphene devices fabricated without the use of resist films by a unique combination of (i) direct patterning by focused ion beam and (ii) contact metallization by direct-write ALD of Pt. The device fabrication steps are shown schematically in Figure 1. We use electrical measurements to demonstrate good device performance in terms of field-effect mobility, and investigate the intrinsic properties of resist-free metal-graphene contacts. The devices show clear evidence for contact-induced doping and unexpected strong Pt-graphene coupling, which is explained by the reduced impact of resist residue under the contacts, the high quality of the Pt-graphene contact interface obtained by direct-write ALD, and the formation of a graphitic interlayer that improves the bonding between the Pt and the graphene. Finally, we speculate that controlling the properties of this interlayer may offer much needed control over the metal-graphene coupling strength and the ability to tune contact properties as desired.

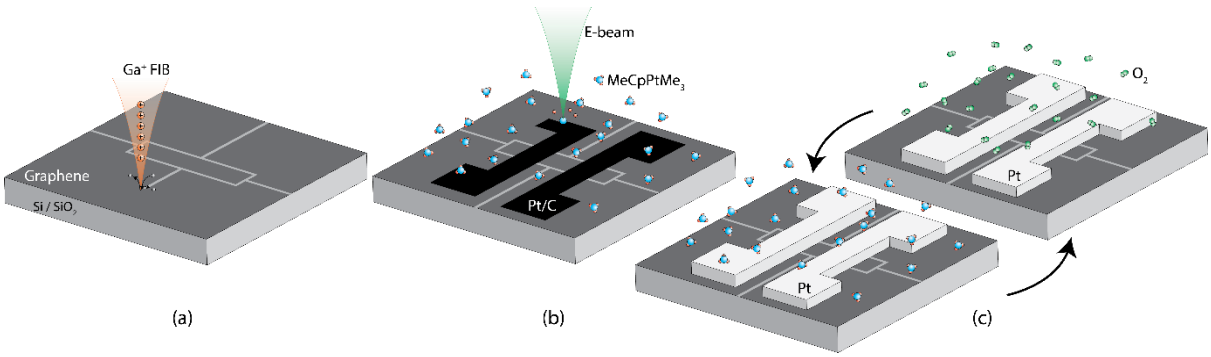

Figure 1. Schematic depiction of the three steps in the resist-free device fabrication process. (a) Directly patterning cuts into the large-area graphene by Ga FIB to define the central channel region. (b) Local deposition of the Pt/C contact pattern seed layer by EBID. (c) Area-selective Pt ALD by cycle-wise and alternating exposure to $MeCpPtMe_3$ and O_2 gas to transform the seed layers into pure Pt contacts.

Methods

Graphene - Large-area graphene was grown by chemical vapor deposition (CVD) and then transferred to a 90 nm SiO_2 / Si substrate using a standard polymethyl methacrylate (PMMA) transfer process.[41] The Si substrate is highly *p*-doped and acts as a back-gate in electrical measurements.

Resist-free fabrication – The resist-free fabrication of graphene devices consists of the following steps which are depicted schematically in Figure 1: (a) defining and isolating the channel region by directly patterning the graphene with a focused ion beam (FIB), (b and c) direct-write ALD of Pt to contact the graphene device channel. Both steps avoid the use of resist films. An FEI Helios 650 DualBeam system was used to pattern the graphene by Ga FIB. Small cuts of about 500 nm in width are patterned with an ion dose of 10 C/m^2, which is sufficient to electrically isolate the channel region.[32] The FIB process was optimized to prevent damage to the graphene in the channel by scattered ions as described elsewhere.[32] In the same DualBeam system, the contact pattern seed layers were then deposited by a standard Pt EBID process using $MeCpPtMe_3$ precursor. Typical electron beam settings include an acceleration voltage of 5 kV, beam current of 20 nA and total electron dose of 1.2 $nC/\mu m^2$. Finally, a home built ALD reactor was used to selectively deposit Pt on the contact seed layers by 500 cycles of an area-selective ALD process, using $MeCpPtMe_3$ and O_2 gas precursors at a substrate table temperature of 300 °C. More details about the direct-write ALD process are available in the Supporting Information and in previous publications.[37–39]

Electrical characterization – Electrical characterization was carried out in a Janis micro-manipulated vacuum probe station, using a Keithley 4200-SCS parameter analyzer. Samples were annealed overnight at 475 K in vacuum (~10^{-4} mbar) to desorb contaminants from the graphene and reduce the ambient doping of the graphene. Measurements were carried out in vacuum after cooling the sample down to room temperature.

Results

Fabrication – The resist-free process for the fabrication of transfer length method (TLM) devices is depicted schematically in Figure 1 and described in detail in the Methods. Figure 2 illustrates the various stages of the resist-free fabrication process by scanning electron microscopy (SEM) and optical images. Figure 2 (a) shows the graphene after FIB patterning of the device regions. The central rectangle defines the device channel, while the remaining cuts serve to electrically isolate all contacts from each other and from the bulk of the graphene. Figure 2 (b) shows an example of a seed layer deposited by EBID, before it is transformed into pure Pt. As is typical for EBID, the seed layer contains ~85% carbon and therefore shows dark contrast.[38,39] Finally, Figure 2 (c) and (d) show a completed device (after electrical measurements) where the area-selective ALD process has turned the seed layers into high-quality Pt.[37,39] From our previous work,[39] the thickness of the carbon-containing EBID seed layer (before ALD) deposited with a similar electron dose (~1 nC/μm^2) is known to be approximately 8 nm, and it contains approximately 85% carbon. However, exposure to oxygen gas during the ALD process purifies the seed layers by combusting the carbon. After ALD, the seed layer is no longer distinguishable as a separate layer and the contacts consist of pure Pt all the way down to the substrate.[39] The final thickness of the contacts is estimated to be approximately 22 nm in these devices. Additional information about the purification of the seed layers in relation to our previous work can be found in the Supporting Information.

Some unintentional Pt deposition can sometimes be observed in the regions where the FIB was used to remove the graphene, most clearly where the contacts cross the FIB cuts. This may be caused by oxygen vacancies in the SiO_2 substrate created by the FIB exposure, which activate the substrate and may cause the Pt precursor to adsorb or decompose.[42,43] However, the deposition does not cause short-circuiting since it is in the form of disconnected particles and does not extend across the entire FIB cut (see Supporting Information).

Since graphene is very sensitive to irradiation from ion and electron beams,[32,44–47] it is important to ensure that the FIB, EBID and ALD processes are not damaging the graphene. Figure 3 (a) shows a Raman spectrum of the smallest channel of a completed device, compared to the spectrum of the same graphene before device fabrication. The presence of only a small D-peak shows that damage in the graphene is minimal, but not completely prevented. Figure 3 (b) shows a map scan of the D peak intensity across the device channels. As expected, the graphene is damaged around the FIB cuts, but the damage is reduced to background levels within 1 μm. There is no change in D peak intensity around the contacts indicating that the EBID and ALD processes do not damage the graphene channels.

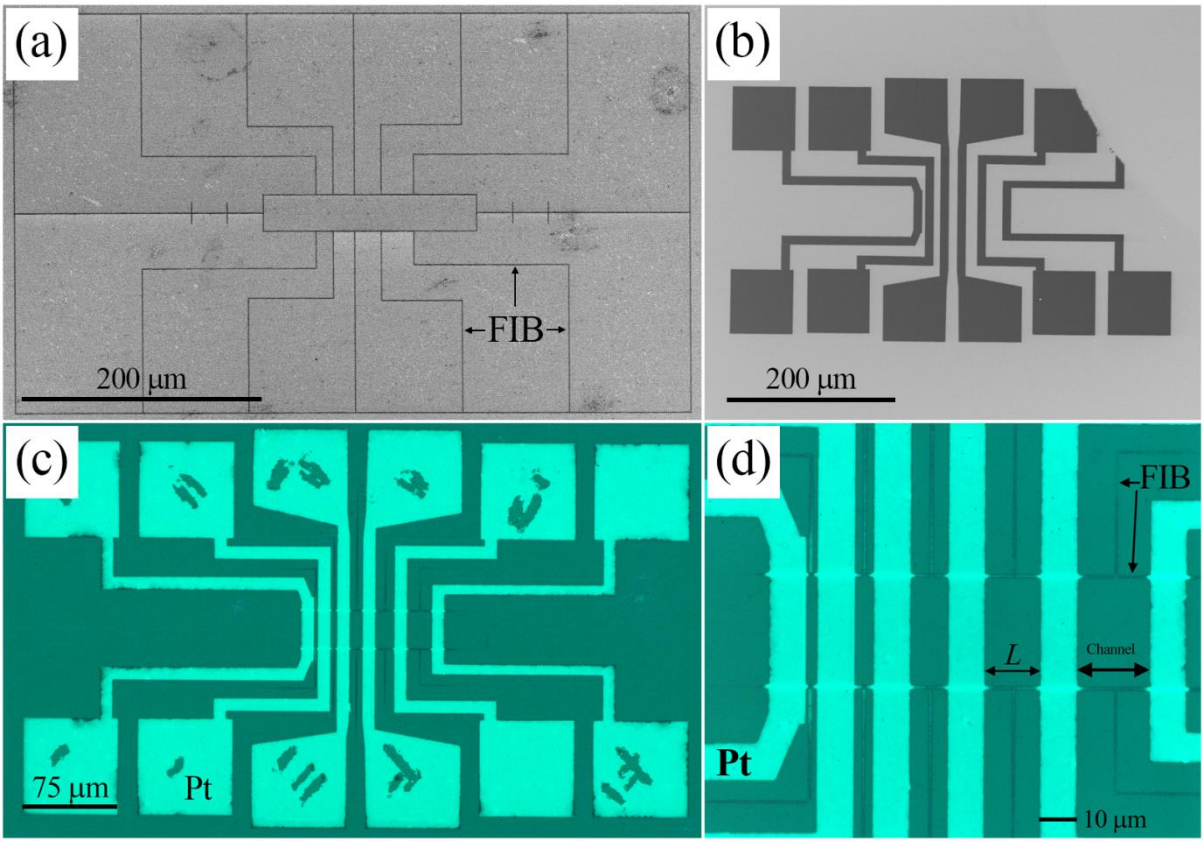

Figure 2. (a) SEM image of the CVD graphene after device channel definition using FIB cuts. (b) SEM image of Pt/C contact seed layers deposited by EBID, before thickening and purification by ALD (the gas injection system was blocking the top-right corner due to misalignment). The dark contrast is caused by the high amount of carbon (~85%). (c) Optical microscope image of a completed device after contact deposition by ALD. The scratches in the Pt originate from probe needles used during the measurements. (d) Zoom-in of the channel region of the same device, where L depicts the channel length of one channel.

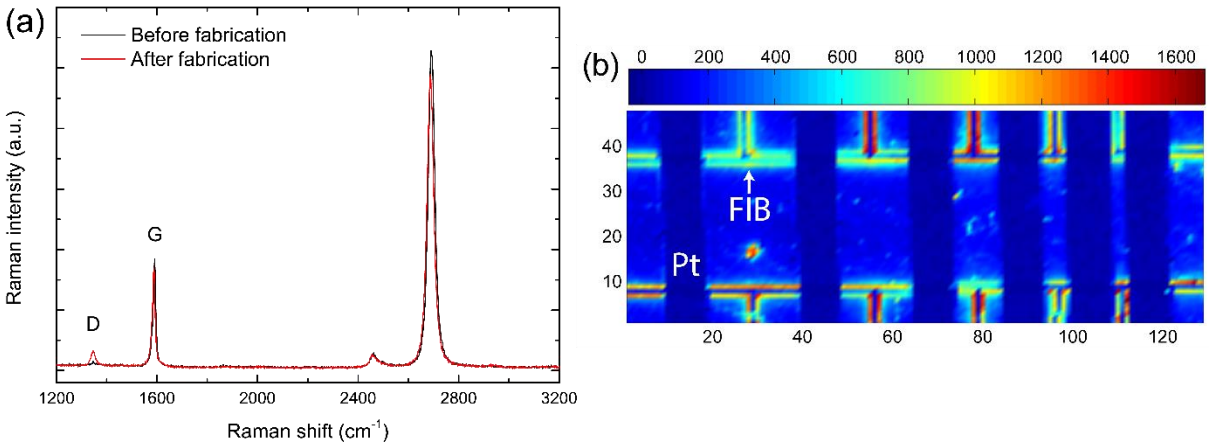

Figure 3. (a) Raman spectrum of the graphene before and after device fabrication measured in the center of the smallest channel. A small D-peak is present indicating a minimal amount of damage during fabrication. (b) Map of the Raman D peak intensity across all device channels, indicating that the graphene is only damaged around the FIB cuts but not in the channel or around the contacts. The contacts are visible as low intensity areas because the Raman signal is much weaker when measured through the Pt. The distance scales are in μm and colorbar scale is absolute intensity.

Device quality – The graphene devices were electrically characterized to confirm that they operate as typical graphene devices and to assess their electrical performance. Since we used a 2-probe measurement configuration, the electrical measurements include contact resistance (which is an important device property) but also a parasitic series resistance from the metal leads (paths from the large "contact pads" to the channel). This parasitic metal lead resistance is small and negligible in typical devices. However, due to the long length of the paths in the devices in this work the metal lead resistance is not negligible and contributes about 330 – 650 Ω depending on the channel measured. Since the metal lead resistance is not relevant for the device properties, the data in Figure 4 has been corrected for contribution of the metal lead resistance as described in the Supporting Information. Any contact resistance however is still present in the data.

Figure 4 (a) shows the output characteristics for each of the 5 consecutive channels (of length L) of a typical device. The drain current I_D is plotted as a function of the drain-source voltage V_{DS} and shows a linear behaviour in the measured range of 0 – 0.1 V. The drain current decreases at longer channel lengths due to an increasing contribution of the channel resistance.

Figure 4 (b) shows the transfer characteristics of the same device (data for the remaining devices is shown in the Supporting Information). The two-probe device resistance is shown as a function of the back-gate voltage V_{GS} for the five consecutive channels. The devices behave as typical graphene devices, with the resistance peaking at the Dirac point V_{Dirac}, which is located at positive gate voltage for every channel due to some residual channel doping by the ambient. Two interesting features are visible: (i) the location of the Dirac point shifts to higher gate voltages as the channel length decreases, and (ii) the curves are asymmetrical with a higher resistance on the positive gate voltage side of the Dirac point ($V_{GS} > V_{Dirac}$). Both features can be explained by the presence of contact induced doping effects, which will be discussed in detail later.

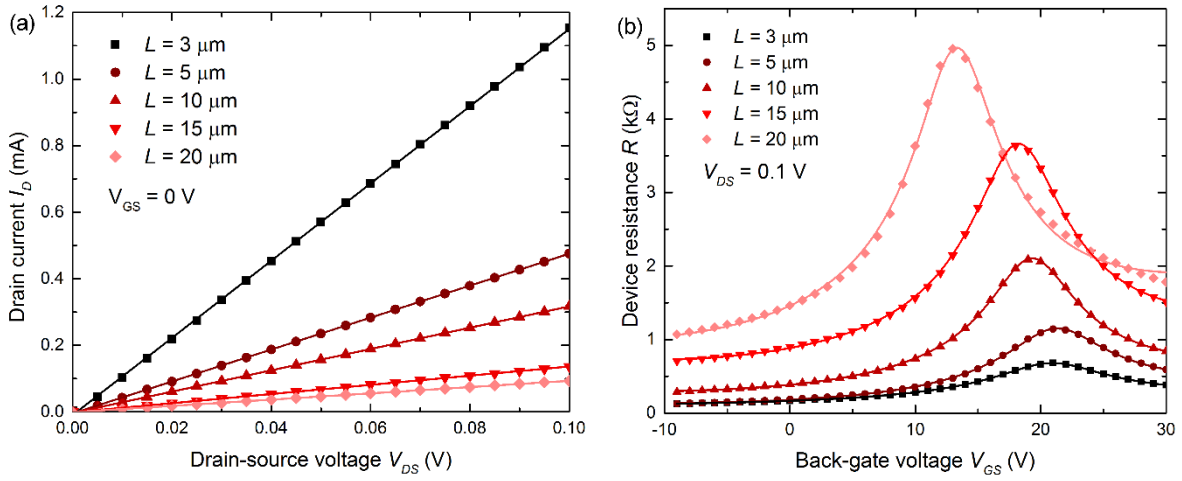

Figure 4. (a) Output characteristics of a typical device (device "3") showing linear V_{DS}-I_D behaviour in the measured range for the 5 consecutive channels with length L. The data has been corrected for the metal lead resistance. Solid lines are linear fits. (b) Transfer characteristics of the same device as (a), showing the 2-probe device resistance as a function of back-gate voltage for the 5 consecutive channels. The data has been corrected for the metal lead resistance. Solid lines are numerical fits using Equation (1).

The transfer characteristics in Figure 4 (b) can be used to extract the field-effect mobility μ of devices by fitting the device resistance R with the commonly used model in Equation (1), as proposed by Kim *et al.*[48]:

$$R(V_{GS}) = 2R_C + \frac{L}{W e \mu \sqrt{n_0^2 + \left[\frac{\varepsilon_{SiO_2}(V_{GS} - V_{Dirac})}{e\, t_{ox}}\right]^2}} + \alpha(V_{GS} - V_{Dirac}) + \beta(V_{GS} - V_{Dirac})^2 \quad (1)$$

Here, W and L are the channel width and length, ε_{SiO_2} is the permittivity of the gate dielectric of thickness t_{ox} and e is the electronic charge. The additional term quadratic in $V_{GS} - V_{Dirac}$ with fit parameters α and β fits the asymmetry of the data as proposed by Di Bartolomeo *et al.*[49] The field-effect mobility μ, the contact resistance R_C, the intrinsic charge carrier density at the Dirac point n_0, and the gate voltage of the Dirac point V_{Dirac} are used as the remaining fit parameters.

The resulting fits are shown using the solid lines in Figure 4 (b), and the extracted field-effect mobility μ is shown in Figure 5 as a function of the channel length for several representative devices. The mobility ranges between ~1000 to ~1800 $cm^2\ V^{-1}s^{-1}$ and varies from device to device, possibly due to graphene quality variation. We do not observe a clear trend in channel length dependence, as expected for these length scales.[50] These mobilities are similar to typical CVD graphene devices[51–54] and are the same as mobilities obtained by large-scale van der Pauw measurements on similar graphene layers, indicating that the devices are performing well.

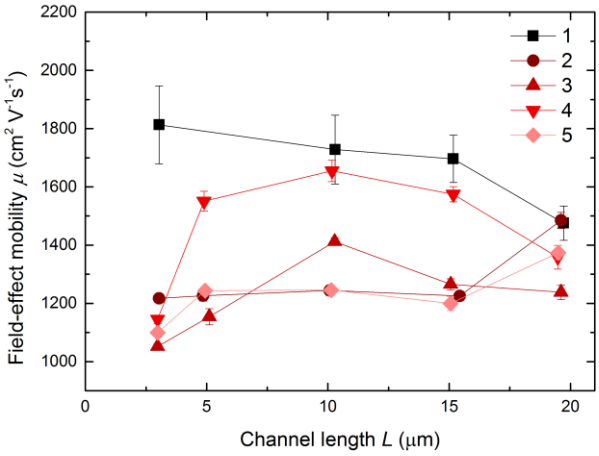

Figure 5. Field-effect mobility μ as a function of the channel length for five devices (1-5), ranging from about 1000 to 1800 $cm^2 V^{-1}s^{-1}$.

Contact resistance – The contact resistance R_C of the Pt direct-write ALD contacts was measured by employing the transfer length method (TLM). At each gate voltage, the device resistance (corrected for the metal lead resistance) is extracted from the transfer characteristics of the five consecutive channels and plotted against the channel length L. The device resistance R should depend linearly on the channel length (assuming diffusive transport and homogenous sheet resistivity ρ of all channels), while the intercept at extrapolated $L = 0$ should yield the contact resistance according to $R(L) = 2R_C + \rho L / W$, where W is the channel width. Figure 6 (a) shows the resulting plot of a representative device for a number of different gate voltages. Extrapolating the resistance by linear fits clearly shows an apparently negative contact resistance. Like the shift of the Dirac point and the asymmetry of the transfer characteristics discussed earlier, the extraction of an apparently negative contact resistance is another observation that can be caused by contact induced doping.[8,55]

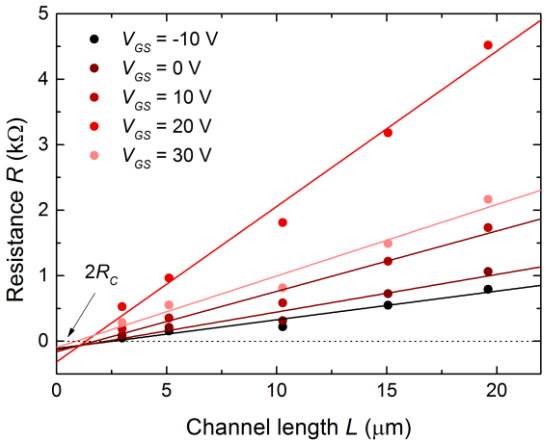

Figure 6. Transfer length method (TLM) measurement of a representative device ("3"), showing the device resistance as a function of the channel length L (for several different gate voltages) to extract the contact resistance at $L = 0$.

Discussion

When graphene is contacted by metallic contacts, a charge transfer occurs in order to equilibrate the work function difference between the metal and graphene. Because the density of states (DOS) in graphene is very low (especially compared to the metal contacts), a small charge transfer leads to a large shift in the Fermi level of the graphene,[20,21] not only under the contacts but extending some distance L_D into the channel.[22] Effectively the contacts dope the graphene near the contacts with either electrons (*n*-type) or holes (*p*-type), with the strength and polarity depending not only on work function difference, but also on the metal-graphene distance due to chemical interaction.[20,21] However, the type of charge carriers in the bulk of the channel is controlled by the electrostatic gate potential. When the type of charge carriers induced electrostatically by the gate is different than the type of charge carriers induced by the contacts, a *p*-*n* junction forms near the contacts which increases the device resistance, see Figure 7 (a). As a result of the *p*-*n* junction the device transfer characteristics become asymmetrical. For example, if the contacts induce hole doping the *p*-*n* junction forms for gate voltages $V_{GS} > V_{Dirac}$ and the resistance is higher on the positive side of the Dirac point. The asymmetry can be clearly observed in Figure 4 (b), and it can be further quantified by calculating the "odd resistance", which is the difference in the device resistance on both sides of the Dirac point. The odd resistance is shown in the Supporting Information and quantifies that there is indeed a higher resistance for $V_{GS} > V_{Dirac}$ in these devices, indicating that the contacts show hole doping behaviour. Hole doping is expected for Pt contacts due to its high work function.[20,21] Additionally, we previously observed a similar effect in carbon nanotubes contacted by Pt direct-write ALD.[56]

The contact induced doping also shifts the Dirac point, as is observed in Figure 4 (b). The shift becomes more apparent as the channel length is decreased, as a relatively larger part of the channel is doped. The direction of the shift can be used to determine the type of contact

doping[24]: electron (hole) doping shifts the Dirac point to more negative (positive) gate voltages when the channel length is decreased. The Dirac point shift for the Pt direct-write ALD contacted devices is plotted as a function of the channel length in Figure 7 (b). Apart from one outlier (device "5"), all devices show a significant shift to more positive gate voltages for smaller channels, which is another indication of hole doping from the Pt to the graphene. According to Ifuku *et al*[19], the doping length L_D may be extracted from the data in Figure 7 (b) as an exponential fit parameter. However, no exponential behavior is observed for these devices, therefore the doping length could not be estimated.

Finally, the extraction of apparently negative contact resistance when using invasive contacts (crossing the entire channel) is also attributed to contact doping effects.[8,55] If the contact quality is high and the contact doping effect is strong, the additional doping extending into the channel effectively changes the channel resistance (even at the Dirac point). This lowers the contact resistance as measured by e.g. TLM, and apparently negative contact resistances can occur when the effect exceeds the actual contact resistance. Therefore, in this case it is impossible to accurately measure the actual contact resistance, even with other popular geometries such as four-point probe measurements. While this is beyond the scope of this work, the contact doping effects can be excluded by using non-invasive contacts.[14,22]

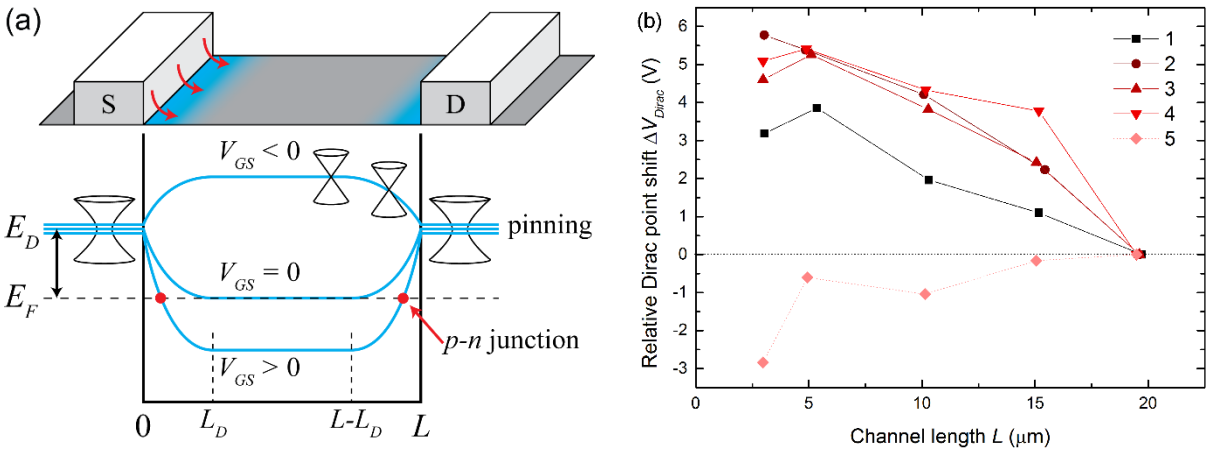

Figure 7. (a) Band diagram of a graphene channel with contact induced doping indicated by the separation between Dirac point E_D and Fermi level E_F (in case of hole doping). The doping extends a distance L_D into the channel. For positive V_{GS}, a *p-n* junction increases the device resistance causing asymmetry in the transfer characteristics. (b) Shift of the Dirac point ΔV_{Dirac} (relative to the longest channel) for five representative devices (1-5). For every device except "5", the Dirac point shifts to higher gate voltages when the channel length is decreased.

The graphene devices demonstrated in this work show clear evidence of strong metal-graphene coupling strength and substantial hole doping from the Pt ALD contacts to the graphene: a shift of the Dirac point as function of the channel length, asymmetrical transfer characteristics and apparently negative contact resistance as measured by TLM. We identify three mechanisms that may explain the observed results. (i) First of all, the resist-free fabrication substantially reduces the amount of resist residue between the contacts and the graphene. Even though some resist residue may be present from the graphene transfer process, the subsequent steps do not add additional residue. This results in a cleaner contact interface, a reduced metal-graphene distance and a larger coupling strength between the Pt and graphene.[19] (ii) Secondly, the direct-write ALD metallization potentially improves the wettability of the Pt to the graphene due to the chemical nature of the technique compared to physical sputtering. As an example, we have recently shown that carbon nanotubes (CNTs) contacted by direct-write ALD of Pt show an improved wettability.[56] While conventional Pt contacts to CNTs typically yield bad wettability to the CNT, resulting in poor device performance (compared to e.g. Pd contacts), Pt direct-write ALD contacts yield device

performance comparable to Pd. (iii) Finally, the deposition of a Pt/C seed layer by EBID (before its subsequent transformation to Pt by ALD) can influence the bonding of the Pt to the graphene. Even though the bulk of the contacts are transformed to pure Pt and the EBID seed layer is no longer distinguishable after ALD,[39] it is likely that a very thin graphitic interlayer remains at the Pt-graphene interface. While Pt itself typically physisorbs very weakly to graphene,[20,21] the graphitic interlayer may result in much stronger chemisorption (larger coupling strength), as has been shown previously for both graphene[57] and carbon nanotubes.[58]

The three mechanisms discussed all influence the coupling strength between the metal and graphene, and the contact induced doping from the metal to the graphene. The metal-graphene coupling is crucially important because it effects the density of states (DOS) in the graphene under the contacts. When the metal-graphene coupling is strong, the DOS under the contacts distorts and increases especially at the charge neutrality point,[17,19] depicted schematically in Figure 7 (a). In this case the larger density of carriers screens a gate potential, and the Fermi level under the contacts cannot be modulated by the gate.[17,59] The Fermi level is effectively pinned, resulting in the formation of a *p-n* junction on one side of the Dirac point and asymmetrical transfer characteristics. A weak coupling on the other hand leaves the conical DOS of pristine graphene mostly intact.[20,21] Due to the vanishing DOS a small charge transfer already results in a large Fermi level shift. The Dirac point can therefore be modulated by the back-gate potential relatively freely even under the contacts.[16,17] For this reason, weakly coupled contacts often show a secondary resistance peak in the transfer characteristics.[15,17,60–62] The main peak still originates from the minimum conductivity in the channel (line up between Fermi level and Dirac point in the channel), while a secondary peak originates from the lineup of the Fermi level and the Dirac point under the contacts, which happens at a different gate potential. The secondary peak may become unobservable if it is too

broad or overlaps with the main peak. This happens when the metal-graphene coupling is strong, or if the contact induced doping is too small[17]. The devices in this work show a large contact induced doping effect, but the transfer characteristics do not show a secondary resistance peak. This indicates that the Pt-graphene coupling is relatively strong. It should be noted that it is not immediately clear whether weak or strong metal-graphene coupling is preferred. For very weakly coupled contacts, the minimum contact length required for highly transmissive contacts (low contact resistance) becomes larger[17], which hinders device scaling. Interestingly however, very strongly coupled contacts also lead to an increase in device resistance due to an overlap between the main and secondary resistance peaks[17]. Therefore, ideally the coupling strength should be controlled to find the best compromise, e.g. weak enough to allow sufficient contact induced doping, but at the same time strong enough to avoid the requirement of large contact lengths. The Pt/C seed layer in the direct-write ALD metallization scheme provides a unique approach to possibly control the metal-graphene coupling. For example, the coupling may be influenced by the thickness and the composition of the seed layer (controlled by EBID process parameters), or by varying process conditions such as purification of the seed layers prior to the ALD step.[39] So far the seed layer properties have been chosen only on the basis of obtaining nucleation of the selective ALD process, and a study of their influence on the electrical properties of devices is left for future work.

Conclusions

In conclusion, we have demonstrated resist-free fabrication of graphene devices. The graphene device channels were patterned directly by focused ion beam (FIB). Metallization was performed by direct-write ALD in which seed layers (deposited by EBID) are transformed into pure Pt by an area-selective ALD process. The use of resist films was avoided in both steps, such that the impact of resist residue is significantly reduced. The fabricated devices

show good performance with typical graphene transfer characteristics and field-effect mobilities ranging from approximately 1000 – 1800 $cm^2 V^{-1}s^{-1}$ as is typical for supported CVD graphene. Furthermore, despite the typically expected weak bonding for Pt, the devices show clear evidence of strong Pt-graphene coupling and substantial contact induced hole doping from the Pt to the graphene. These effects are likely caused by the reduced amount of resist residue under the contacts, the improved wettability of the ALD metal and the formation of an atomically thin graphitic interlayer between the Pt and graphene as a result of the EBID seed layer. Furthermore, the seed layer may be a unique approach to controlling the metal-graphene coupling by simply changing its thickness and composition.

Acknowledgements

The authors would like to thank A. Franklin (Duke University) and Z. Chen (Purdue University) for fruitful discussions on graphene devices. We thank P. Trompenaars, R. Geurts and P. Faber (FEI Company) for assistance, helpful discussions and access to their systems. We thank C. van Bommel, J. Meulendijks, J. van Gerwen and J. Zeebregts for technical assistance. This work was financially supported by NWO and the Technology Foundation STW through the VIDI program on "Novel bottom-up nanofabrication techniques for future carbon-nanoelectronics".

References

[1] Geim A and Novoselov K 2007 The rise of graphene. *Nat. Mater.* 183–91

[2] Bolotin K I, Sikes K J, Jiang Z, Klima M, Fudenberg G, Hone J, Kim P and Stormer H L 2008 Ultrahigh electron mobility in suspended graphene *Solid State Commun.* **146** 351–5

[3] Morozov S V., Novoselov K S, Katsnelson M I, Schedin F, Elias D C, Jaszczak J A and Geim A K 2008 Giant intrinsic carrier mobilities in graphene and its bilayer *Phys. Rev. Lett.* **100** 11–4

[4] Castro Neto A H, Guinea F, Peres N M R, Novoselov K S and Geim A K 2009 The electronic properties of graphene *Rev. Mod. Phys.* **81** 109–62

[5] Schwierz F 2010 Graphene transistors. *Nat. Nanotechnol.* **5** 487

[6] Lee E J H, Balasubramanian K, Weitz R T, Burghard M and Kern K 2008 Contact and edge effects in graphene devices *Nat. Nanotechnol.* **3** 486–90

[7] Huard B, Stander N, Sulpizio J A and Goldhaber-Gordon D 2008 Evidence of the role of contacts on the observed electron-hole asymmetry in graphene *Phys. Rev. B - Condens. Matter Mater. Phys.* **78**

[8] Blake P, Yang R, Morozov S V, Schedin F, Ponomarenko L A, Zhukov A A, Nair R R, Grigorieva I V, Novoselov K S and Geim A K 2009 Influence of metal contacts and charge inhomogeneity on transport properties of graphene near the neutrality point *Solid State Commun.* **149** 1068–71

[9] Xia F, Perebeinos V, Lin Y, Wu Y and Avouris P 2011 The origins and limits of metal-graphene junction resistance. *Nat. Nanotechnol.* **6** 179–84

[10] Smith J T, Franklin A D, Farmer D B and Dimitrakopoulos C D 2013 Reducing contact resistance in graphene devices through contact area patterning *ACS Nano* **7** 3661–7

[11] Leong W S, Gong H and Thong J T L 2014 Low-contact-resistance graphene devices with nickel-etched-graphene contacts *ACS Nano* **8** 994–1001

[12] Gong C, McDonnell S, Qin X, Azcatl A, Dong H, Chabal Y J, Cho K and Wallace R M 2014 Realistic metal-graphene contact structures *ACS Nano* **8** 642–9

[13] Chari T, Ribeiro-Palau R, Dean C R and Shepard K L 2016 Resistivity of rotated graphite-graphene contacts *Nano Lett.* acs.nanolett.6b01657

[14] Cadore A R, Mania E, de Morais E A, Watanabe K, Taniguchi T, Lacerda R G and Campos L C 2016 Metal-graphene heterojunction modulation via H_2 interaction *Appl. Phys. Lett.* **109** 33109

[15] Karnatak P, Sai T P, Goswami S, Ghatak S, Kaushal S and Ghosh A 2016 Current crowding mediated large contact noise in graphene field-effect transistors *Nat. Commun.*

7 13703

[16] Chen Z C Z and Appenzeller J 2009 Gate modulation of graphene contacts - on the scaling of graphene FETs *2009 Symp. VLSI Technol.* 128–9

[17] Knoch J, Chen Z and Appenzeller J 2012 Properties of metal-graphene contacts *IEEE Trans. Nanotechnol.* **11** 513–9

[18] Moriyama T, Nagashio K, Nishimura T and Toriumi A 2013 Carrier density modulation in graphene underneath Ni electrode *J. Appl. Phys.* **114**

[19] Ifuku R, Nagashio K, Nishimura T and Toriumi A 2013 The density of states of graphene underneath a metal electrode and its correlation with the contact resistivity *Appl. Phys. Lett.* **103** 33514

[20] Giovannetti G, Khomyakov P A, Brocks G, Karpan V M, Van Den Brink J and Kelly P J 2008 Doping graphene with metal contacts *Phys. Rev. Lett.* **101** 4–7

[21] Khomyakov P A, Giovannetti G, Rusu P C, Brocks G, Van Den Brink J and Kelly P J 2009 First-principles study of the interaction and charge transfer between graphene and metals *Phys. Rev. B - Condens. Matter Mater. Phys.* **79** 1–12

[22] Nagashio K, Nishimura T, Kita K and Toriumi A 2009 Metal/graphene contact as a performance Killer of ultra-high mobility graphene - Analysis of intrinsic mobility and contact resistance *Tech. Dig. - Int. Electron Devices Meet. IEDM* 565–8

[23] Mueller T, Xia F, Freitag M, Tsang J and Avouris P 2009 Role of contacts in graphene transistors: A scanning photocurrent study *Phys. Rev. B - Condens. Matter Mater. Phys.* **79** 1–6

[24] Nouchi R, Saito T and Tanigaki K 2011 Determination of carrier type doped from metal

contacts to graphene by channel-length-dependent shift of charge neutrality points *Appl. Phys. Express* **4**

[25] Chaves F A, Jiménez D, Cummings A W and Roche S 2014 Physical model of the contact resistivity of metal-graphene junctions *J. Appl. Phys.* **115**

[26] Song S M and Cho B J 2013 Contact resistance in graphene channel transistors *Carbon Lett.* **14** 162–70

[27] Suk J W, Lee W H, Lee J, Chou H, Piner R D, Hao Y, Akinwande D and Ruoff R S 2013 Enhancement of the electrical properties of graphene grown by chemical vapor deposition via controlling the effects of polymer residue *Nano Lett.* **13** 1462–7

[28] Lin Y, Lu C, Yeh C, Jin C, Suenaga K and Chiu P 2012 Graphene Annealing: How Clean Can It Be? *Nano Lett.* **12** 414–9

[29] Chavarin C A, Sagade A A, Neumaier D, Bacher G and Mertin W 2016 On the origin of contact resistances in graphene devices fabricated by optical lithography *Appl. Phys. A Mater. Sci. Process.* **122** 1–5

[30] Nath A, Koehler A D, Jernigan G G, Wheeler V D, Hite J K, Hernández S C, Robinson Z R, Garces N Y, Myers-Ward R L, Eddy C R, Gaskill D K and Rao M V. 2014 Achieving clean epitaxial graphene surfaces suitable for device applications by improved lithographic process *Appl. Phys. Lett.* **104** 224102

[31] Ghoneim M T, Smith C E and Hussain M M 2013 Simplistic graphene transfer process and its impact on contact resistance *Appl. Phys. Lett.* **102**

[32] Thissen N F W, Vervuurt R H J, Mulders J J L, Weber J W, Kessels W M M and Bol A A 2015 The effect of residual gas scattering on Ga ion beam patterning of graphene

Appl. Phys. Lett. **107**

[33] Kim K, Lee H-B-R, Johnson R W, Tanskanen J T, Liu N, Kim M-G, Pang C, Ahn C, Bent S F and Bao Z 2014 Selective metal deposition at graphene line defects by atomic layer deposition. *Nat. Commun.* **5** 4781

[34] Wang X, Tabakman S M and Dai H 2008 Atomic layer deposition of metal oxides on pristine and functionalized graphene *J. Am. Chem. Soc.* **130** 8152–3

[35] Park K S, Kim S, Kim H, Kwon D, Koo Lee Y-E, Min S-W, Im S, Choi H J, Lim S, Shin H, Koo S M and Sung M M 2015 Wafer-scale single-domain-like graphene by defect-selective atomic layer deposition of hexagonal ZnO *Nanoscale* **7** 17702–9

[36] Vervuurt R H J, Sharma A, Jiao Y, Kessels W (Erwin) M M and Bol A A 2016 Area-selective atomic layer deposition of platinum using photosensitive polyimide *Nanotechnology* **27** 405302

[37] Mackus A J M, Mulders J J L, van de Sanden M C M and Kessels W M M 2010 Local deposition of high-purity Pt nanostructures by combining electron beam induced deposition and atomic layer deposition *J. Appl. Phys.* **107** 116102

[38] Mackus A J M, Dielissen S A F, Mulders J J L and Kessels W M M 2012 Nanopatterning by direct-write atomic layer deposition *Nanoscale* **4** 4477–80

[39] Mackus A J M, Thissen N F W, Mulders J J L, Trompenaars P H F, Verheijen M A, Bol A A and Kessels W M M 2013 Direct-write atomic layer deposition of high-quality Pt nanostructures: Selective growth conditions and seed layer requirements *J. Phys. Chem. C* **117** 10788–98

[40] Botman A, Mulders J J L and Hagen C W 2009 Creating pure nanostructures from

electron-beam-induced deposition using purification techniques: a technology perspective *Nanotechnology* **20**

[41] Kasry A, Kuroda M A, Martyna G J, Tulevski G S and Bol A A 2010 Chemical doping of large-area stacked graphene films for use as transparent, conducting electrodes *ACS Nano* **4** 3839–44

[42] Walz M M, Schirmer M, Vollnhals F, Lukasczyk T, Steinrück H P and Marbach H 2010 Electrons as "Invisible Ink": Fabrication of nanostructures by local electron beam induced activation of SiOx *Angew. Chemie - Int. Ed.* **49** 4669–73

[43] Kubena R L 1988 Selective area nucleation for metal chemical vapor deposition using focused ion beams *J. Vac. Sci. Technol. B Microelectron. Nanom. Struct.* **6** 1865

[44] Ferrari A and Robertson J 2000 Interpretation of Raman spectra of disordered and amorphous carbon *Phys. Rev. B* **61** 14095–107

[45] Lucchese M M, Stavale F, Ferreira E H M, Vilani C, Moutinho M V O, Capaz R B, Achete C a. and Jorio a. 2010 Quantifying ion-induced defects and Raman relaxation length in graphene *Carbon N. Y.* **48** 1592–7

[46] Fox D, Zhou Y B, O'Neill A, Kumar S, Wang J J, Coleman J N, Duesberg G S, Donegan J F and Zhang H Z 2013 Helium ion microscopy of graphene: beam damage, image quality and edge contrast. *Nanotechnology* **24** 335702

[47] Pan C T, Hinks J A, Ramasse Q M, Greaves G, Bangert U, Donnelly S E and Haigh S J 2014 In-situ observation and atomic resolution imaging of the ion irradiation induced amorphisation of graphene *Sci. Rep.* **4** 6334

[48] Kim S, Nah J, Jo I, Shahrjerdi D, Colombo L, Yao Z, Tutuc E and Banerjee S K 2009

Realization of a high mobility dual-gated graphene field-effect transistor with Al2O3 dielectric *Appl. Phys. Lett.* **94**

[49] Di Bartolomeo A, Giubileo F, Romeo F, Sabatino P, Carapella G, Iemmo L, Schroeder T and Lupina G 2015 Graphene field effect transistors with niobium contacts and asymmetric transfer characteristics *Nanotechnology* **26** 475202

[50] Chen Z and Appenzeller J 2008 Mobility extraction and quantum capacitance impact in high performance graphene field-effect transistor devices *Technical Digest - International Electron Devices Meeting, IEDM* (IEEE) pp 1–4

[51] Kedzierski J, Hsu P, Reina A, Kong J, Healey P, Wyatt P and Keast C 2009 Graphene on Insulator Transistors Made Using C on Ni Chemical Vapor Deposition *Phys. Rev.* **30** 2–4

[52] Pirkle A, Chan J, Venugopal A, Hinojos D, Magnuson C W, McDonnell S, Colombo L, Vogel E M, Ruoff R S and Wallace R M 2011 The effect of chemical residues on the physical and electrical properties of chemical vapor deposited graphene transferred to SiO_2 *Appl. Phys. Lett.* **99** 122108

[53] Chan J, Venugopal A, Pirkle A, McDonnell S, Hinojos D, Magnuson C W, Ruoff R S, Colombo L, Wallace R M and Vogel E M 2012 Reducing extrinsic performance-limiting factors in graphene grown by chemical vapor deposition *ACS Nano* **6** 3224–9

[54] Franklin A D, Han S J, Bol A A and Perebeinos V 2012 Double contacts for improved performance of graphene transistors *IEEE Electron Device Lett.* **33** 17–9

[55] Nouchi R, Saito T and Tanigaki K 2012 Observation of negative contact resistances in graphene field-effect transistors *J. Appl. Phys.* **111**

[56] Mackus A J M, Thissen N F W, Chen Z H, Trompenaars P H F, Mulders J J L, Kessels W M M and Bol A A 2016 Resist-free fabricated carbon nanotube field-effect transistors with high-quality atomic-layer-deposited platinum contacts *Appl. Phys. Lett.* Accepted for publication

[57] Kim S, Russell M, Kulkarni D D, Henry M, Kim S, Naik R R, Voevodin A A, Jang S S, Tsukruk V V. and Fedorov A G 2016 Activating "Invisible" Glue: Using Electron Beam for Enhancement of Interfacial Properties of Graphene–Metal Contact *ACS Nano* acsnano.5b06342

[58] Chai Y, Hazeghi A, Takei K, Chen H Y, Chan P C H, Javey A and Wong H S P 2012 Low-resistance electrical contact to carbon nanotubes with graphitic interfacial layer *IEEE Trans. Electron Devices* **59** 12–9

[59] Nouchi R and Tanigaki K 2010 Charge-density depinning at metal contacts of graphene field-effect transistors *Appl. Phys. Lett.* **96** 1–4

[60] Di Bartolomeo A, Giubileo F, Santandrea S, Romeo F, Citro R, Schroeder T and Lupina G 2011 Charge transfer and partial pinning at the contacts as the origin of a double dip in the transfer characteristics of graphene-based field-effect transistors. *Nanotechnology* **22** 275702

[61] Feng T, Xie D, Xu J, Zhao H, Li G, Ren T and Zhu H 2014 Back-gate graphene field-effect transistors with double conductance minima *Carbon N. Y.* **79** 363–8

[62] Zhang C, Xie D, Xu J L, Li X M, Sun Y L, Dai R X, Li X and Zhu H W 2015 HfO2 dielectric thickness dependence of electrical properties in graphene field effect transistors with double conductance minima *J. Appl. Phys.* **118**